Int. J. Electrochem. Sci., 15 **(2020)** 10509 – 10523, doi: 10.20964/2020.10.44

International Journal of
ELECTROCHEMICAL
SCIENCE
www.electrochemsci.org

Effect of carbon nanodots supported palladium-based electrocatalysts towards oxygen reduction reaction in an alkaline medium

T.A. Mashola[1], *T. Matthews*[1], *L.T. Dlamini*[1], *N.W. Maxakato*[1*]

Department of Chemical Sciences, University of Johannesburg, Doornfontein, 2028, South Africa.
[*] E-mail: nmaxakato@uj.ac.za

Received: 25 May 2020 / *Accepted:* 10 July 2020 / *Published:* 31 August 2020

Carbon nanodots (CNDs) have been synthesised using a simple and cheap pyrolysis method. The Pd/CNDs electrocatalyst was synthesised by the in-situ reduction method. The calculated particle sizes were found to be 6.0 nm and 0.974 nm for CNDs and Pd nanoparticles, respectively. The reaction kinetics of the Pd/CNDs was found to have an onset potential of -0.111 V, which is 0.052 V lower than that of Pd/C. CNDs are good electrocatalysts support, as supported by durability and stability studies. The electrocatalyst showed improved durability and stability when CNDs were used as the support material for the Pd nanoparticles.

Keywords: carbon nanodots, electro-catalysis, oxygen reduction reaction, electrode, fuel cells

1. INTRODUCTION

Carbon materials possess interesting physical and structural properties that make them suitable for application in fuel cells. These include their low cost, large surface area, and good electrical conductivity. Many carbon materials have been synthesised and used as standalone electrocatalysts and support materials for catalysts [1], [2]. Carbon nanodots (CNDs) are one-dimensional quasi-spherical nanomaterials with sizes less than 10 nm. They have variable structures and compositions, exhibiting interesting optical and photochemical properties [3], [4], [5]. This carbonaceous nanomaterial is divided into two groups, namely, amorphous carbon nanoparticles and crystalline lattice carbon quantum dots [3], [6]. There are two methods for the synthesis of CNDs, the top-down and bottom-up methods. The top-down method involves treatment of larger carbon materials, such as graphite powder and carbon nanotubes in harsh chemical conditions. The bottom-up approach involves the application of external energy, such as microwaves [7], [8], [9], pyrolysis [10], ultrasonication and hydrothermal treatment of small carbon-containing materials, such as starch [11], sweet potatoes [12], citric acid [13], [14], waste

paper [15], ascorbic acid [16], peony flower [17], and glucose [18], [19], [20] to form carbon nanomaterial. Carbon nanodots were first discovered by Scrivens and co-workers. [21] through purification of single-wall carbon nanotubes (SWCNTs). Since their discovery, they have attracted tremendous research attention, due to their desirable properties [4]. CNDs have also been used in many applications, ranging from catalysis to bio-imaging. In this report, carbon nanodots have been used as electrocatalysts support for oxygen reduction catalytic material in alkaline media.

Alkaline fuel cells (AFCs) represent one of the promising green energy alternatives for the 21st century that will help mitigate the lack of energy supply, environmental pollution and global warming resulting from the burning of fossil fuels for energy production [8], [10]. The use of liquid as an electrolyte and low-temperature operation make AFCs much cheaper and easy to operate. AFCs also have high cell voltages resulting from higher reaction kinetics than acidic conditions, enabling the use of a lower quantity of the catalysts [22]. One of the major reactions that occur in the fuel cell for the production of electricity is the reduction of oxygen at the cathode. This process can occur in two ways, the slow two-electron transfer pathway involving the production of the intermediate product hydrogen peroxide that can poison the electrocatalyst and the fast reaction involving direct four-electron transfer to produce water [23]. Currently, a platinum catalyst is used for the electro-catalysis of these reactions, but, due to many drawbacks, such as platinum cost and scarcity surrounding the use of platinum, fuel-cell commercialisation has been hindered [13], [14]. In addition to platinum drawbacks, other hindrances are low durability, and nanoparticles agglomeration or leaching from the carbon support, leaving the support vulnerable to oxidation or corrosion, which reduces fuel cell performance and lifetime.

Electrode performance and lifetime are also affected by the tolerance of Pt catalyst for poisoning [10], [13], [15], [16]. In addition, fuel cells also have a lower conversion efficiency than theoretically predicted, which results from the sluggish oxygen-reduction reaction at the cathode, even on platinum which is considered the best catalyst [18], [19], [24]. Previous studies have shown that about 70% of energy losses are accounted for by the overpotential for oxygen reduction reactions at the cathode [1]. Because the reduction of oxygen is slower than the oxidation of hydrogen, the overall energy output is directly linked to the cathodic reaction, due to polarisation losses at the cathode [25]. In this sense, there is a remarkable interest in developing Pt-free cathode materials that will enhance the catalysis of oxygen to improve fuel cell activity, stability and lifetime, while reducing the catalyst cost. Electrode catalyst activity is the primary factor of the electrochemical performance of fuel cells [26]. Previous studies have shown that, except for platinum, palladium is the best metal catalyst for oxygen reduction reaction [10], [22]. In addition to its catalytic behaviour, palladium is much cheaper and more abundant in the earth's crust than platinum. The specific activity of catalysts is related to the support material. This study was aimed at developing catalyst support material for the enhancement of catalytic activity and stability of the electrocatalyst for oxygen reduction reaction (ORR) in alkaline media.

2. MATERIALS AND METHODS

2.1 Chemicals

All reagents used were of analytical grade: Palladium (II) chloride (Aldrich), sodium borohydride (UniLAB), potassium hydroxide (Sigma), alumina powder (Buehler), nafion solution 20% (Sigma), ethanol > 99.9% (Sigma-Aldrich), and potassium bromide (Sigma-Aldrich).

2.2 Synthesis of carbon nanodots

Carbon nanodots (CNDs) were synthesised following a method reported by Shi and co-workers, [10]. Briefly, oats were pyrolyzed in a muffle furnace at 400˚C for 2 hrs. The black product was cooled to room temperature and then crushed to a fine powder. The powder was dispersed in distilled water and centrifuged for 15 min to remove larger particles. The obtained CNDs aqueous suspension was filtered and the CNDs powder was obtained after drying in an oven at 80˚C overnight.

2.3 Synthesis of Pd/CNDs electrocatalyst

The Pd/CNDs electrocatalyst was synthesised using the in-situ reduction method. CNDs was dispersed in distilled water to form a CNDs aqueous solution. The palladium chloride solution was added to the CNDs suspension and the solution was refluxed for 30 min, followed by the addition of a reducing agent and finally refluxed for 2 hrs. A 0.1 M $NaBH_4$ was the reducing agent. The suspension was centrifuged and the resulting slurry was washed with distilled water and dried at ambient temperature overnight.

2.4 Characterisation

TEM (JEOL 2100 HRTEM 200 kV, Japan) was used to obtain images for the morphology and particle size studies. Image J software was used for average particle size estimation. XRD (X'Pert Philips) with a monochromatic Cu Kα (0.1540 nm) generated at 40 kV and 40 mA was used to investigate the crystalline structure and particle size of the Pd/CNDs electrocatalyst. Bruker Alpha FTIR Fourier-Transform Infrared Spectroscopy (FTIR) was used for the identification of functional groups. A WiTeC confocal Raman spectrometer was used to determine the structural and morphological properties of the electrocatalysts at an excitation wavelength of 531.77 nm. XPS Kratos Axis Ultra DLD, using an Al (monochromatic) anode, equipped with a charge neutraliser was used to determine the elemental composition, oxidation states and surface functional groups.

2.4 Electrochemical measurements

The working electrode modification was carried out as prescribed by the work of Gwebu and co-workers [27]. The commercial 10 wt.% Pd/C electrocatalyst was prepared similarly and all

electrochemical measurements were conducted at room temperature. The electrolyte solutions were purged with argon gas and oxygen gas for 20 min prior to the experiment.

3. RESULTS AND DISCUSSION

3.1 Morphology, particle size and size distribution: TEM

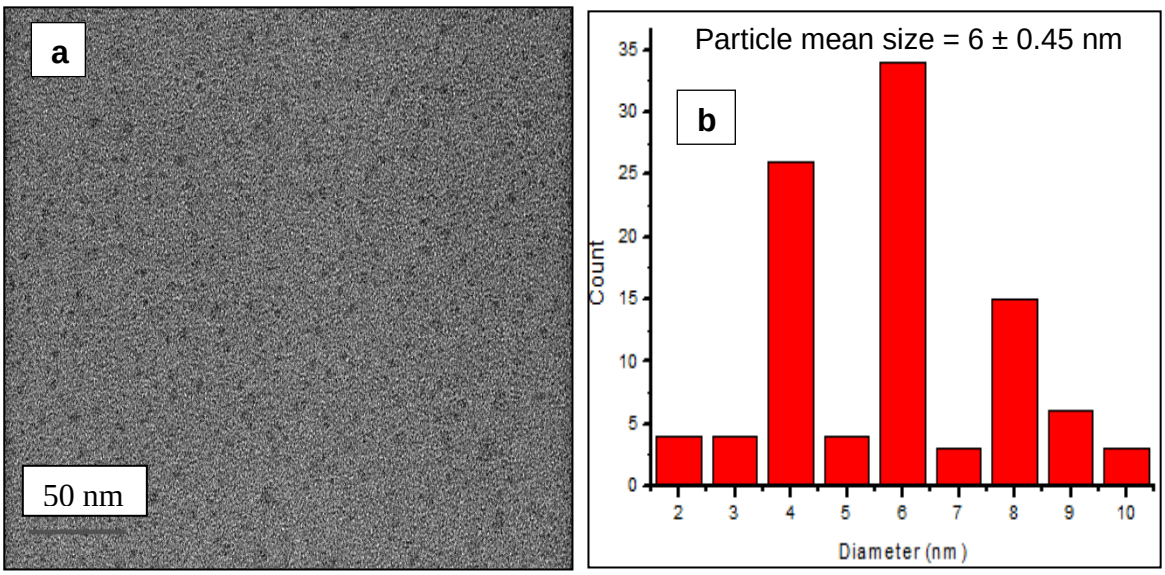

Figure 1. (a) TEM images of CNDs and (b) particle size distribution

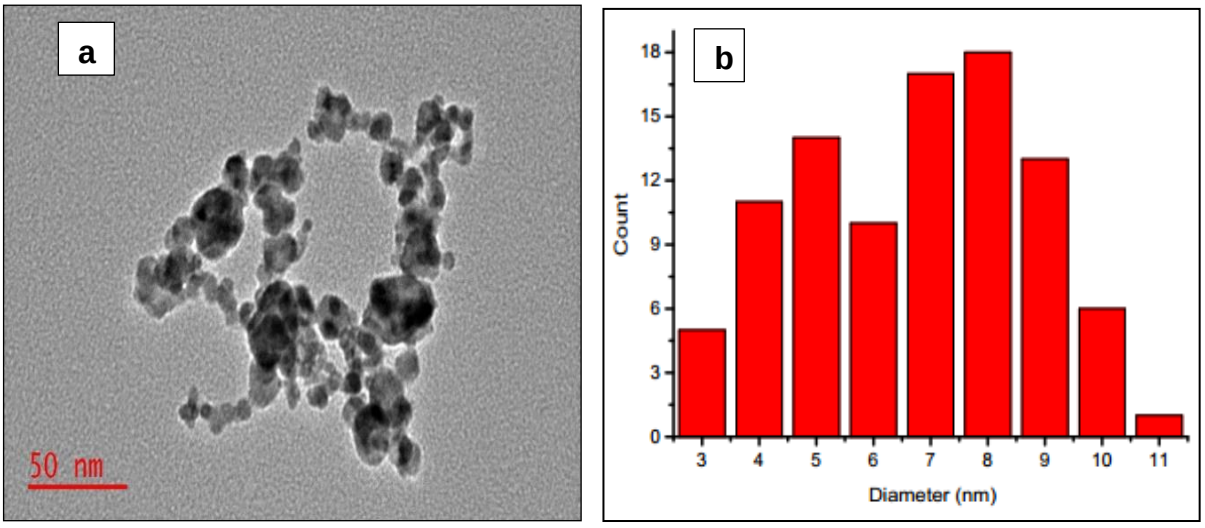

Figure 2. (a) TEM images of Pd/CNDs and (b) particle size distribution

Particle size and morphology have a significant influence on the electrochemical activity of electrocatalysts. As shown in Fig. 1 (a), the CNDs are well dispersed in a spherical shape. Fig. 1 (b) shows that the synthesised CNDs are very small, in the range 2 – 10 nm, with a mean of 6 ± 0.45 nm. This was much smaller than the particle size obtained by Shi and co-workers. [10], which had a particle size distribution of 7 – 11 nm and a mean size of 8.64 ± 0.84 nm. Fig. 2 shows that the synthesised

Pd/CNDs electrocatalyst was well-dispersed with spherical shapes. The particle sizes for Pd/CNDs electrocatalyst was found to be in the range 3 – 10 nm, with a mean size of 7 ± 0.86 nm.

3.2 FTIR spectral characterisation of CNDs

Surface-oxygen moieties based functional groups of the support material are of great significance for the incorporation of the metal nanoparticles to the support material. FTIR spectroscopy was used for the determination of surface functional groups of the CNDs, as shown in Fig. 3. The FTIR spectrum of CNDs shows peaks at 3424 and 2925 cm^{-1}, which are attributed to the O-H and C-H stretching vibrations, while the peaks at 1399 and 1602 cm^{-1} are indicative of the existence of carbonyl and carbon-carbon π bonds from the graphitic structure of the CNDs. The disappearance of the peak at 1399 cm^{-1} in the Pd/CNDs spectrum is indicative of the successful incorporation of Pd nanoparticles to the surface of the CNDs support. The peaks at 1108 and 1036 cm^{-1} are ascribed to the C-O and C-O-C stretching vibrations respectively.

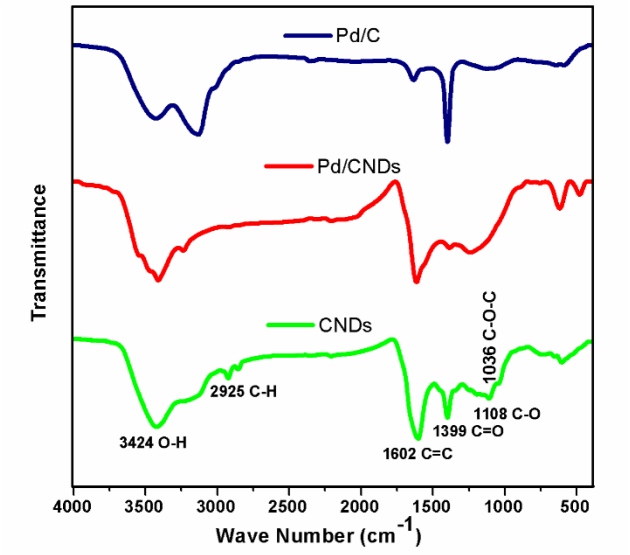

Figure 3. FTIR spectra of the Pd/C, Pd/CNDs and CNDs

3.3 X-ray powder diffraction

XRD analysis is an important tool to determine the crystallinity of an electrocatalyst. Fig. 4 shows the XRD spectra of CNDs support material and Pd/CNDs electrocatalyst. The diffraction peak at 25° in both the XRD patterns is from the (002) planes of the carbon nanodots support material. The diffraction peak at 25° (002) and 43° (100) from the CNDs spectrum is also an indication of impurity-free graphite-like structures [24], [28]. The diffraction peaks in Pd/CNDs monometallic electrocatalyst spectrum observed at 40°, 46°, 68°, 82° and 86° are the characteristics of a face-centred, cubic structure of Pd crystal with crystalline planes (111), (200), (220), (311) and (222) respectively [28], [29], [30]. The

average particle size calculated from the XRD of the Pd (111) diffraction peak using the Scherrer equation $L = \frac{K \times \lambda}{b\cos\theta}$, was estimated to be 0.974 nm.

Where D is the average crystallite size, K is the Scherrer constant (typical value ~ 0.9), λ is the wavelength of the X-ray (0.154178 nm), and β is the line broadening at half the maximum intensity.

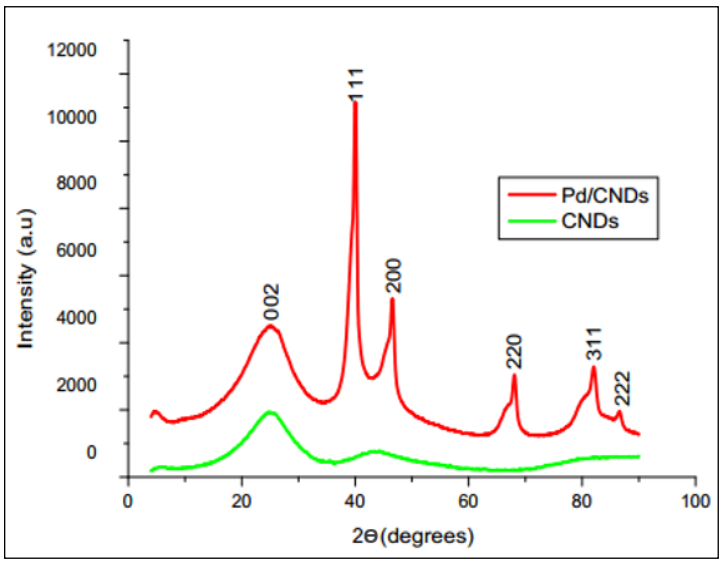

Figure 4. XRD spectra of CNDs and Pd/CNDs

3.4 Raman spectroscopy

Raman spectroscopy is used to characterise the order of the crystalline structure of carbon-based materials. In this study, Raman spectra were used to determine the order of the structure of naked CNDs and CNDs as support in Pd/CNDs electrocatalyst, as shown in Fig. 5. Raman spectra obtained for CNDs and Pd/CNDs electrocatalyst in the region 800 – 2000 cm^{-1} are shown in Fig. 5. In both samples, two prominent peaks were displayed around 1355 cm^{-1} and 1590 cm^{-1}, which were assigned to the D (A_{1g} symmetry) and G (E_{2g} symmetry) bands respectively. The D band is the breathing mode of k-point phonons and is associated with the local defects in the nanomaterials and the G band refers to the sp^2-bonded carbon-atom vibrations [30], [31]. The G-band upward shift in Pd/CNDs compared to CNDs (Table 1) is due to the higher disorder of CNDs in Pd/CNDs than in CNDs. Disordered solids usually have G bands that are shifted to higher Raman wave numbers than the ordered ones [30]. The ratio of the D to G band peak intensity was used to measure the size of the sp^2 carbon clusters and the formation of defects on the surface of the nanomaterials. The ratios were found to be 0.981 and 0.966 for Pd/CNDs and CNDs, respectively. The higher I_D/I_G value of Pd/CNDs than CNDs indicates that the incorporation of Pd to CNDs caused defects in the CNDs structure and lattice symmetry. The I_D/I_G was also used to assess the in-plane crystalline size (L_a), a measure of the inter-defect distance. The following equation was used to calculate L_a:

$$L_a \text{ (nm)} = 2.4 \times 10^{-10} \lambda^4 I_G/I_D$$

λ is the wavelength of the laser in nm [30]. From the in-plane crystalline sizes, the high L_a of CNDs (Table 1) shows a decrease in the crystallite size of CNDs in Pd/CNDs compared to naked CNDs, but not to a great extent.

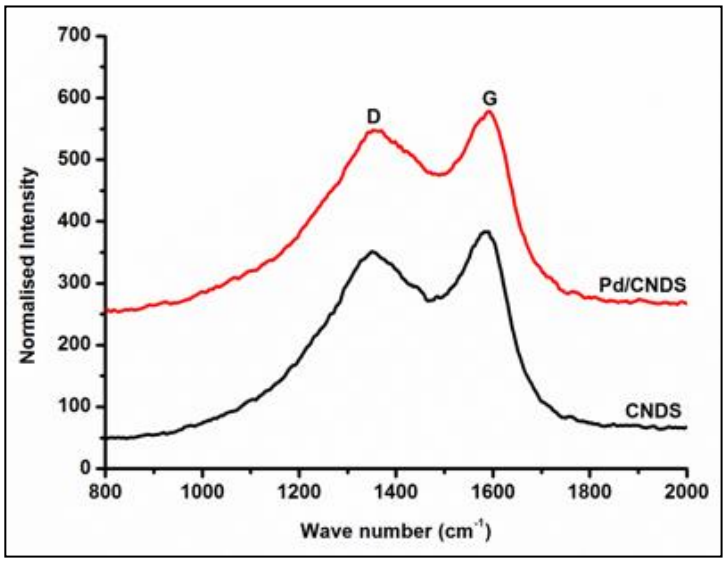

Figure 5. Raman spectra of CNDs and Pd/CNDs

Table 1. Raman parameters obtained from Raman spectra of CNDs and Pd/CNDs.

Carbon and carbon-based nanomaterials	V_D (cm^{-1})	V_G (cm^{-1})	I_D/I_G	L_a (nm)
CNDs	1353.3	1589.7	0.9	20.6
Pd/CNDs	1355.6	1592	1	20

*V_D and V_G correspond to the peak positions. I_D and I_G correspond to the peak intensities respectively. $W_1/2_D$ and $W_1/2_G$ correspond to the full width at half-maximum of D and G bands. La represents the in-plane crystallite size and is determined from equation 2.

3.5. XPS Characterisation

The elemental composition, oxidation states and surface functional groups were determined by XPS. Fig. 6 shows the (a) XPS survey spectrum of Pd/CNDs and high-resolution spectra of (b) C 1s, (c) O 1s and (d) Pd 3d. The survey and high resolution (C 1s and O 1s) spectra of CNDs were as discussed in our previous report [27]. After the metal reduction reaction, Pd was deposited onto CNDs. The peak at around 339 eV was attributed to the Pd 3d. The composition of the sample showed C 1s (81.9%), Pd 3d (1.6%), N 1s (2.6%) and O 1s (13.9%). The presence of C 1s, O 1s and N 1s was not surprising as these were also observed on CNDs samples. The presence of Pd 3d confirmed the deposition of Pd onto CNDs and the amount of Pd deposited was about 1.6%. The high-resolution C 1s and O 1s of the CNDs were also discussed in our previous work [27]. In this work, the high resolution of C 1s, O 1s and Pd 3d are be discussed. The high resolution of the C 1s in Fig. 6 (b) for the Pd/CNDs was deconvoluted and

four synthesised peaks were obtained at 284.7 eV (C-C, C=C), 286.0 eV (C-O, C-N), 287.8 eV (C=O, C=N) and 288.8 eV (O=C-O). The NIIST database was used for peak assignments [32]. The high resolution of O 1s in Fig. 6 (c) for the Pd/CNDs were deconvoluted and showed four peaks at 530.6 eV (Pd-O), 532.1 eV (O-H), 533.6 eV (C-O) and 535.3 eV (C-O-C, C=O). The Pd 3d high resolution in Fig. 6 (d) was deconvoluted and three peaks were synthesised at 335.1 eV (Pd^0), 337.1 eV (Pd^{2+}) and 338.1 eV (Pd^{2+}). The Pd 3d high-resolution spectra showed peak-splitting coupling (ΔE) of 5.4 – 6.0 eV typical of the Pd. The oxidation states showed the presence of metallic Pd with zero oxidation with ΔE of 5.4 eV and the Pd with a +2 oxidation state with ΔE of 5.6 eV for the 337.1 eV component and 6.0 eV for the 338.1 eV component. The two +2 palladium oxidation states at 337.1 correspond to Pd-O for the adsorption of palladium onto CNDs. The other +2 oxidation state of Pd at 338.1 eV comes from the metal salt ($PdCl_2$) used for the formation of Pd nanoparticles.

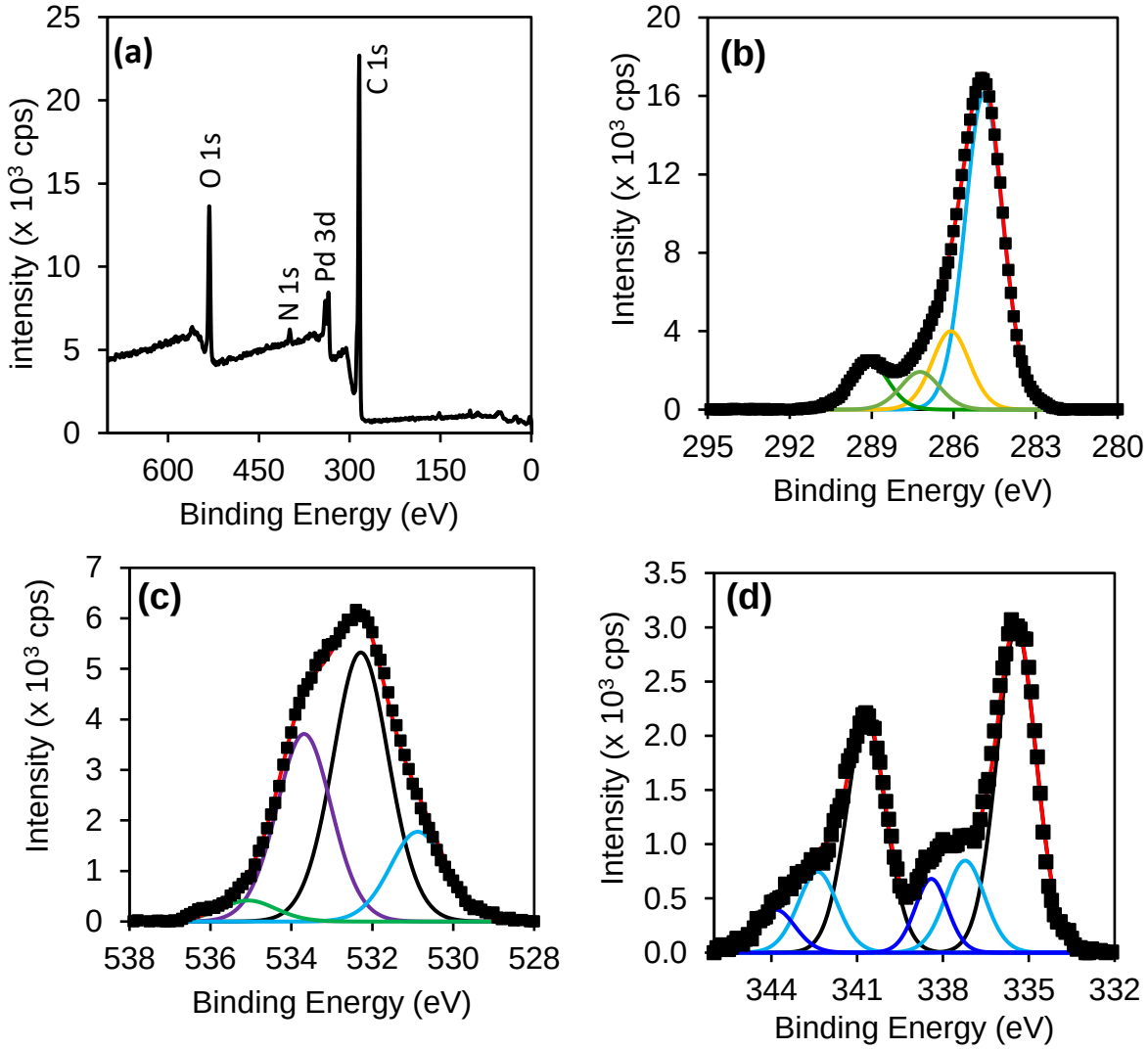

Figure 6. XPS (a) survey spectrum of Pd/CNDs and high-resolution spectra of (b) C 1s, (c) O 1s and (d) Pd 3d.

3.6 Electrochemical analysis

Electrochemical studies were performed to determine the electrocatalytic behaviour of the synthesised electrocatalysts towards oxygen reduction reaction (ORR) in alkaline media and the obtained results were compared to the commercial Pd/C electrocatalyst. The stability and durability of the electrocatalysts were also evaluated.

3.7 Effect of scan rate on oxygen reduction

The reliance of Pd oxide reduction peaks on the scan rates was determined in the range 10 – 100 mV/s, as shown in Fig. 7 (a-b). Voltammetric studies at various scan rates brought about a direct linear relationship between the scan rates and the cathodic peak current values, which is trademark conduct for limited species in the main part of the cathode, showing that the electroactive species are firmly entrapped in the cathode surface. The reduction potential shifts to a more negative value with an increase of scan rate. The Tafel slope was calculated from the slope of E_p vs log v graph, using the equation:

$$E_p = \frac{b}{2}\log V + \text{constant}$$

Where b/2 is the slope of the graph and the Tafel slope is indicated by b [33]. Two distinct slopes are obtained for the graph of commercial Pd/C electrocatalyst, which suggest a change in the mechanism of the oxygen reduction with an increase in scan rate [34]. The slope obtained at low scan rates is b/2=0.061 V/dec, with the Tafel slope of 0.121 V/dec. At high scan rates, the obtained slope was 0.172 V/dec, resulting in the Tafel slope of 0.344 V/dec.

The high Tafel slope value of Pd/C is a characteristic of the porous nature of the electrocatalyst with a high internal surface area [35]. The slope of Ep vs log V was found to be 0.031 of Pd/CNDs electrocatalyst, which resulted with the Tafel slope of 0.062 V/dec, which is lower than both Tafel slopes of the Pd/C plot. High Tafel slopes are also associated with a fast over-potential increase with the current intensity [36]. This indicates good catalytic activity of Pd/CNDs electrocatalyst, which is desirable for electrochemical applications.

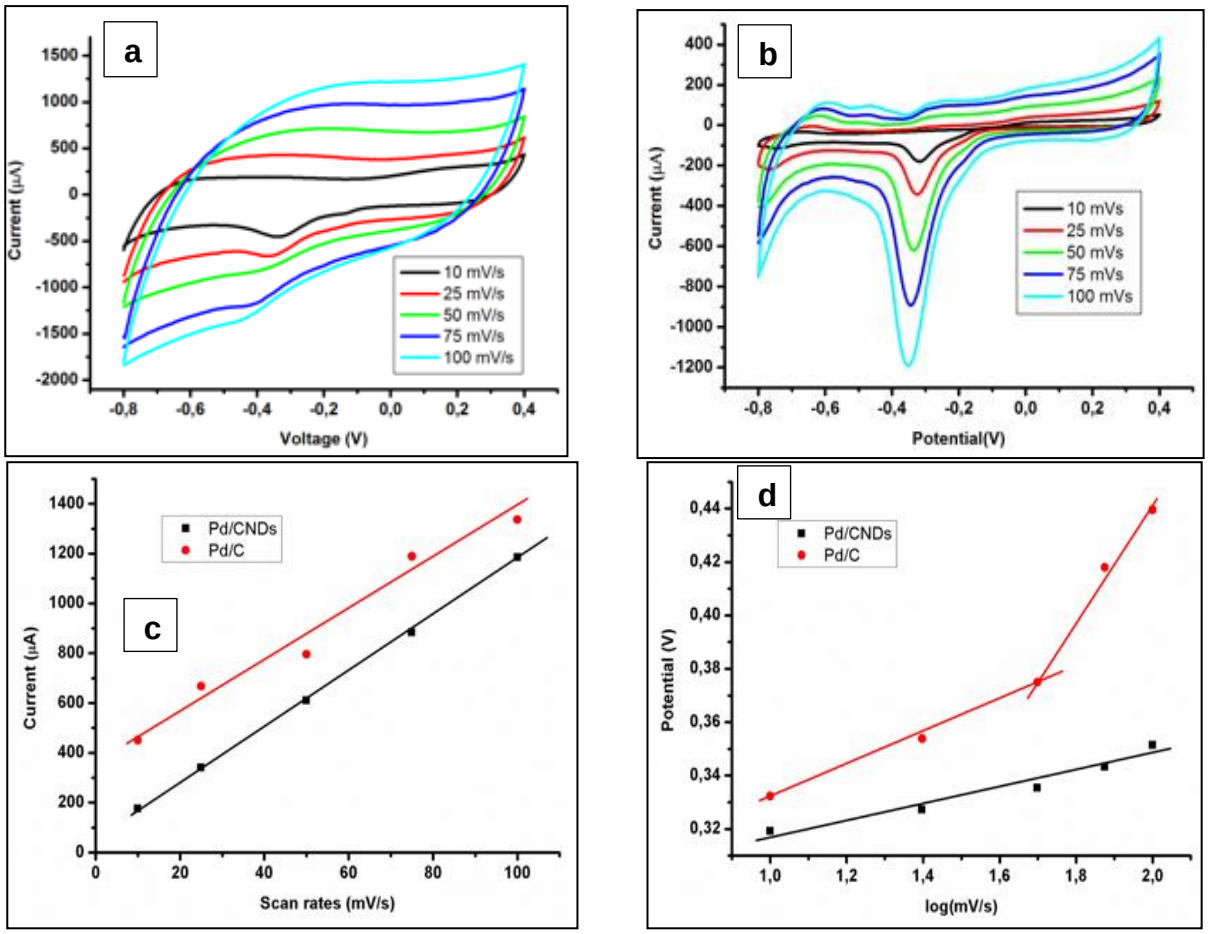

Figure 7. Cyclic voltammograms of (a) Pd/C and (b) Pd/CNDs in O_2-saturated 0.1 M KOH recorded at different scan rates in the range 10 – 100 mV/s, (c) dependence of reduction peak current on scan rates, (d) dependence of reduction peak potential on the logarithmic value of the scan rates (mV/s).

3.8 Comparison of oxygen reduction on Pd/C and Pd/CNDs electrocatalysts: Cyclic voltammetry

Surface characteristics of the electrocatalyst are important factors that determine the activity of the electrocatalyst. To understand this characteristic, oxygen reduction reaction was used as a probe to test the electrocatalytic activity of the CND-supported Pd nanoparticles, in comparison with the electrocatalytic activity of commercial Pd/C electrocatalyst. Cyclic voltammetry (CV) of the synthesised electrocatalyst was recorded in oxygen-saturated 0.1 M KOH, with a scan rate of 50 mV/s. As shown in Fig. 8, the CV curve of Pd/CNDs electrocatalyst showed well-established peaks in the region -0.8 to -0.6 V, a characteristic of the hydrogen adsorption-desorption on the surface of the electrocatalysts, which is consistent with published literature for carbon-supported Pd electrocatalysts in alkaline media [37]. The peak around -0.4 V in both CV of Pd/C and Pd/CNDs electrocatalysts in Fig. 8 is considered to be from the reduction of the oxide layer (Pd-O) to palladium [38], which is also consistent with the reported work [39]. The reaction kinetics of the Pd/CNDs electrocatalyst was found to have an $E_{1/2}$ at -0.336 V and Aeon of -0.111 V. The onset potential of Pd/C electrocatalyst is 0.052 V higher than that of Pd/CNDs electrocatalyst. The electrocatalyst's durability remains one of the main issues that need to be addressed

before its widespread application in fuel cells. In order to determine the durability of the electrocatalysts, continuous potential sweeps between -0.8 V and 0.4V were applied in oxygen-saturated 0.1 M KOH solution for 40 times, as shown in Fig. 9. Upon long-term potential cycling, a slight peak shift and a decrease in peak intensity of Pd-O reduction peaks were observed. The current produced by Pd/CNDs electrocatalyst decreased by 8.32%, which is 2.27% less than the decrease in current produced by Pd/C electrocatalyst. The results show comparable durability of Pd/C and Pd/CNDs electrocatalysts. The high durability of the two electrocatalysts is also associated with the electrolyte medium. The presence of excess OH anions in alkaline medium enhances the development of Pd-OH on the surface, resulting in more stable CV in alkaline than in acidic electrolytes [40]. The slight current decay with an increase in the number of scan rates is probably due to the aggregation of Pd nanoparticles, carbon-support corrosion and Ostwald ripening [41]. Table 3 also indicates the high dependence of the electrocatalytic activity of electrocatalysts on the support material.

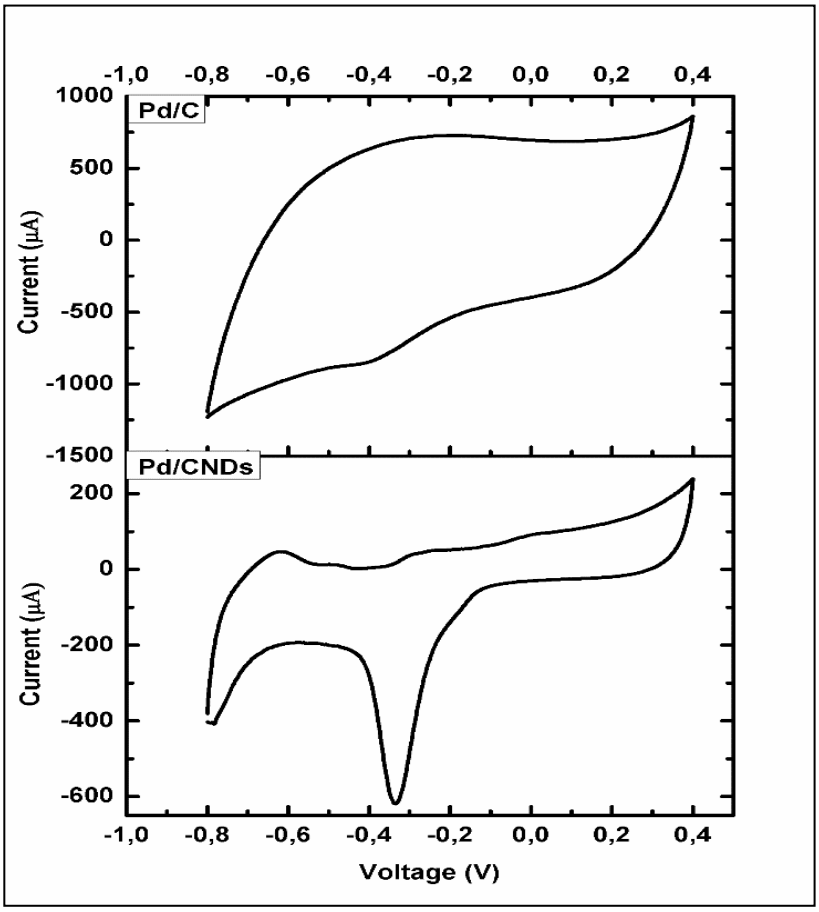

Figure 8. The CV of Pd/C and Pd/CNDs at 50 mV/s in O_2-saturated 0.1 M KOH.

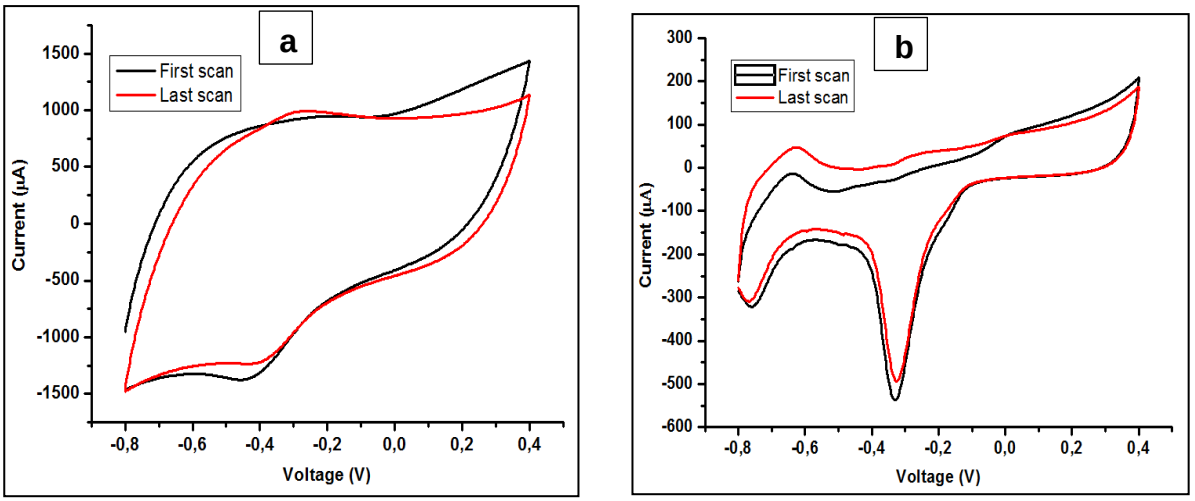

Figure 9. (a) Pd/C and (b) Pd/CNDs durability test at 50 mV/s in O_2-saturated 0.1 M KOH.

Table 2. Comparison of electrochemical performance of Pd/CNDs against other cathode electrocatalysts for oxygen reduction reaction.

Catalysts	$E_{1/2}$	Aeon	Electrode	Medium	References
Pd/C	-0.3893	-0.163.4	Ag/AgCl	Alkaline	Used as standard in this work
Pd/CNDs	-0.3369	-0.111	Ag/AgCl	Alkaline	This work
Pd/MoS_2	-0.2	0.05	Hg/HgO	Alkaline	[42]
Pd/NF	0.377	-	SCE	Acidic	[43]
Pd-Net	0.84	0.925	RHE	Alkaline	[41]
PdNPs	0.78	0.86	RHE	Alkaline	[41]
Pd/RGO	-0.161	0.156	Ag/AgCl	Alkaline	[39]
Pd/rPOM	0.7	1.078	RHE	Alkaline	[44]
Pd tetrapods	0.656	-	RHE	Acidic	[45]
Pd NC/C	0.86	-	RHE	Alkaline	[46]

3.9 Stability studies: Chronoamperometry

For real-life applications, an ideal catalyst must have high catalytic activity, exhibiting high stability and durability. Chronoamperometry was used to determine the stability of the Pd/ CNDs electrocatalyst at 0.35 V for 3600 s in an O_2-saturated 0.1 M KOH solution. Fig. 10 compares the chronoamperometric responses of Pd/CNDs and Pd/C electrocatalysts at oxygen reduction reaction potentials. The prepared catalyst was found to have acceptable stability, higher than that of commercial palladium supported on Vulcan carbon. A steady decrease in the current density was observed in the first few minutes, which then became constant with time, in agreement with the durability results.

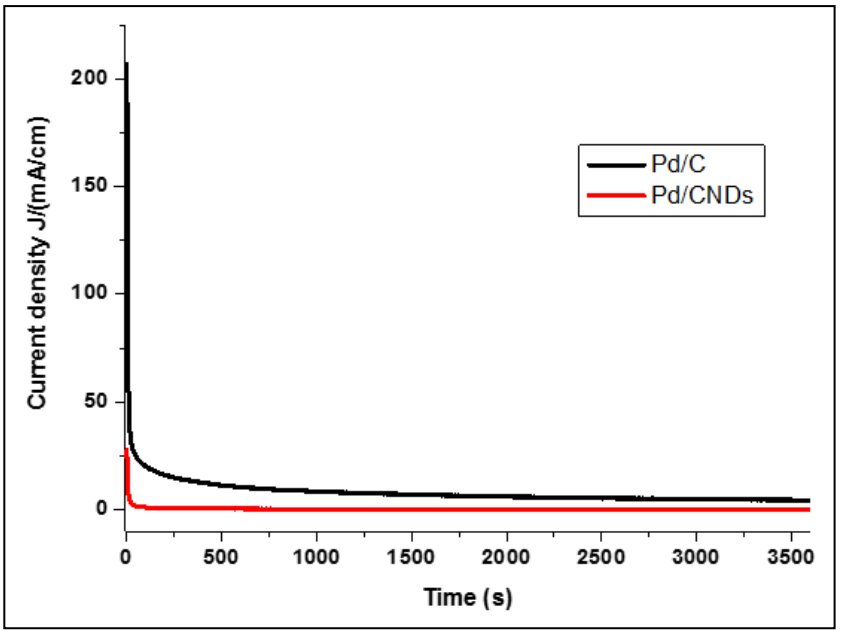

Figure 10. Chronoamperometric detection of Pd/C and Pd/CNDs in O_2-saturated 0.1 M KOH.

4. CONCLUSIONS

A simple and cost-effective method has been used to successfully synthesise an electrocatalyst and electrocatalyst support material. Highly functionalised carbon nanodots (CNDs) were successfully synthesised using a green method. TEM images showed well-dispersed CNDs and the successful incorporation of the Pd nanoparticles onto the surface of the CNDs. FTIR, XRD and XPS measurements clearly confirmed the successful synthesis of Pd/CNDs electrocatalyst. Electrochemical characterisation showed that Pd/CNDs electrocatalyst has higher electrochemical activity compared to commercial Pd/C electrocatalyst for oxygen reduction in an alkaline medium. Improved durability and stability were also observed when CNDs were used as the support material. These results confirm that CNDs are a good electrocatalyst support material with high stability compared to Vulcan carbon, resulting in highly stable electrocatalysts.

DATA AVAILABILITY

Data available on request; please contact Nobanathi W. Maxakato, +27 83 513-4598 nmaxakato@uj.ac.za.

CONFLICTS OF INTEREST

There are no conflicts of interest.

FUNDING STATEMENT

For financial support, the authors are grateful to the University of Johannesburg's Faculty of Science, University Research Council, National Research Foundation of South Africa grant number (TTK 15071-0125-019) and Department of Science and Technology and National Nanoscience Postgraduate Teaching and Training Programme (NNPTTP).

ACKNOWLEDGEMENTS
The Centre for Nanomaterials Science Research, University of Johannesburg, South Africa. The authors gratefully acknowledge the efforts and support provided by the electrochemistry group during the research and preparation of the manuscript.

References

1. Z. Shih, A. P. Periasamy, P. Hsu, and H. Chang, *App. Cat., B,* 133 (2013) 363.
2. M. Yaldagard, N. Seghatoleslami, and M. Jahanshahi, *Appl. Surf. Sci.*, 315 (2014) 222.
3. P. Innocenzi, L. Malfatti, and D. Carboni, *Nanoscale*, 7 (2015) 12759.
4. Y. Park, J. Yoo, B. Lim, W. Kwon, and S.-W. Rhee, *J. Mater. Chem. A*, 4 (2016) 11582.
5. F. Messina, L. Sciortino, R. Popescu, A. M. Venezia, A. Sciortino, G. Buscarino, S. Agnello, R. Schneider, D. Gerthsen, M. Cannas and F. M. Gelardi., *J. Mater. Chem. C*, 4 (2016) 2598.
6. D. Reyes, M. Camacho, M. Camacho, M. Mayorga, D. Weathers, G. Salamo, Z. Wang and A. Neogi, *Nanoscale Res. Lett.*, 11 (2016) 424.
7. Y. Li, P. Miao, W. Zhou, X. Gong, and X. Zhao, *J. Mater. Chem. A*, 5 (2017) 21452.
8. K. Dimos, F. Arcudi, A. Kouloumpis, I.B. Koutselas, P. Rudolf, D. Gournis and M. Prato, *Nanoscale*, 9 (2017) 10256.
9. B. Ninwong, P. Sangkaew, and P. Hapa, RSC Adv., 10 (2020) 9884.
10. L. Shi, X. Li, Y. Li, X. Wen, J. Li, M.M.F. Choi, C. Dong, S. Shuang, *Sens. Actuators, B*, 210 (2015) 533.
11. S. N. A. Mohd Yazid, S. F. Chin, S. C. Pang, and S. M. Ng, *Microchim. Acta*, 180 (2013) 137.
12. W. Lu, X. Qin, A. M. Asiri, A. O. Al-Youbi, and X. Sun, *J. Nanopart. Res.*, 15 (2013) 1344.
13. L. Deng, Wang, Y. Kuang, C. Wang, L. Luo, F. Wang, and X. Sun, *Nano Res.,* 8 (2015) 2810.
14. X. Liu, H-B. Li, L. Shi, X. Meng, Y. Wang, X. Chen, H. Xu, W. Zhang, X. Fang and T. Ding, *J. Mater. Chem. C*, 5 (2017) 10302.
15. A. Fadllan, P. Marwoto, M. P. Aji, and R. S. Iswari, AIP Conf. Proc., 1788 (2017).
16. X. Fang, X. M. Wu, X. L. Hu, Z. J. Li, and G. L. Wang, *Microchim. Acta*, 183 (2016) 2761.
17. J. Gu, X. Li, Z. Zhou, W. Liu, K. Li, J. Gao, Y. Zhao and Q. Wang, *Nanoscale,* 11 (2019) 13058.
18. P. Yang, J. Zhao, J. Wang, B. Cao, L. Li, and Z. Zhu, *J. Mater. Chem. A*, 3 (2015) 8256.
19. M. Liu and W. Chen, *Nanoscale*, 5 (2013) 12558.
20. X. F. Xi, Y. Y. Li, and L. He, *RSC Adv.,* 10 (2020) 411.
21. X. Xu, R Ray, Y. Gu, H. J. Ploehn, L. Gearheart, K. Raker, and W.A. Scrivens, *J. Am. Chem. Soc.,* 126 (2004) 12736.
22. N. R. Nik Roselina and A. Azizan, *Procedia Eng.*, 41 (2012) 1620.
23. L. Zhang and Z. Xia, *J. Phys. Chem. C*, 115 (2011) 1117.
24. P. K. Sonkar, K. Prakash, M. Yadav, V. Ganesan, M. Sankar, R. Gupta and D. K. Yadav, *J. Mater. Chem. A*, 5 (2017) 6263.
25. G. Merle, M. Wessling, and K. Nijmeijer, *J. Membr. Sci.*, 377 (2011) 1.
26. W. Zhang, H. Huang, F. Li, K. Deng, and X. Wang, *J. Mater. Chem. A*, 2 (2014) 19084.
27. S. S. Gwebu, P. N. Nomngongo, P. N. Mashazi, T. Nyokong, and N. W. Maxakato, *Int. J. Electrochem. Sci.*, 12 (2017) 6365.
28. D. Rajesh, P. Indra Neel, A. Pandurangan, and C. Mahendiran, *Appl. Surf. Sci.*, 442 (2018) 787.
29. Y. Holade, C. Canaff, S. Poulin, T. W. Napporn, K. Servat, and K. B. Kokoh, *RSC Adv.*, 6 (2016) 12627.
30. J. Ma, A. Habrioux, Y. Luo, G. Ramos-Sanchez, L. Calvillo, G. Granozzi, P.B. Balbuena and N. Alonso-Vante, *J. Mater. Chem. A*, 3 (2015) 11891.
31. R. Kannan, A. R. Kim, J. S. Kim, and D. J. Yoo, *Int. J. Hydrogen Energy*, 41 (2016) 18033.
32. X. Llovet, D. Bote, and C. J. Powell, "NIST NSRDS 164 NIST Database of Cross Sections for

Inner-Shell Ionization by Electron or Positron Impact.
33. Z. Mojovi, T. Mudrini, and P. Bankovi, *J. Solid State Electrochem.,* 19 (2015) 1993.
34. S. Hebié, M. Bayo-Bangoura, K. Bayo, K. Servat, C. Morais, T. W. Napporn and K. B. Kokoh, *J. Solid State Electrochem.*, 20 (2016) 931.
35. N. W. Maxakato, S. A. Mamuru, and I. Ozoemena, *Electroanalysis*, 23 (2011) 325.
36. H. Q. Dong, Y. Y. Chen, M. Han, S.L Li, J. Zhang, J. S. Li, Y. Q. Lan, Z.H. Dai, J. C. Bao, *J. Mater. Chem. A*, 2 (2014) 1272.
37. M. V. Castegnaro, W.J. Paschoalino, M.R. Fernandes, B. Balke, M. C. M. Alves, E. A. Ticianelli, and J. Morais, *Langmuir*, 33 (2017) 2734.
38. R. M. Abdel Hameed, *J. Colloid Interface Sci.*, 505 (2017) 230.
39. P. Raghavendra, G. V. Reddy, R. Sivasubramanian, P. S. Chandana, and L. S. Sarma, *Int. J. Hydrogen Energy*, 43 (2017) 4125.
40. I. Srejic, Z. Rakocevic, M. Nenadovic, and S. Strbac, *Electrochim. Acta*, 169 (2015) 22.
41. H. Begum, M. S. Ahmed, S. Cho, and S. Jeon, *Int. J. Hydrogen Energy*, 43 (2017) 229.
42. E. Lee and Y. U. Kwon, *RSC Adv.*, 6 (2016) 47468.
43. A. Godinez-Garcia and D. F. Gervasio, *RSC Adv.*, 4 (2014) 42009.
44. X. Xie, Y. Nie, S. Chen, W. Ding, X. Qi, and Z. Wei, *J. Mater. Chem. A*, 3 (2015) 13962.
45. R. Zhao, Y. Liu, C. Liu, G. Xu, Y. Chen, Y. Tang and T. Lu, *J. Mater. Chem. A*, 2 (2014) 20855.
46. J. T. L. Gamler, K. Shin, H. M. Ashberry, Y. Chen, S. L. A. Bueno, Y. Tang, G. Henkelman and S. E. Skrabalak, *Nanoscale,* 12 (2020) 2532